Research article

Changjiu Sun, Junli Wei, Jian Zhao*, Yuanzhi Jiang, Yilong Wang, Haiqing Hu, Xin Wang, Yongqin Zhang* and Mingjian Yuan

Hard and soft Lewis-base behavior for efficient and stable $CsPbBr_3$ perovskite light-emitting diodes

https://doi.org/10.1515/nanoph-2021-0003
Received January 6, 2021; accepted April 15, 2021;
published online May 10, 2021

***Corresponding authors: Jian Zhao**, Key Laboratory of Rubber-Plastics Ministry of Education/Shandong Provincial Key Laboratory of Rubber-Plastics, Qingdao University of Science & Technology, 266042, Qingdao, P. R. China; School of Materials Science and Engineering, Qilu University of Technology (Shandong Academy of Sciences), Jinan 250353, P. R. China; Key Laboratory of Organosilicon Chemistry and Material Technology of Ministry of Education, Hangzhou Normal University, Hangzhou 311121, P. R. China; and State Key Laboratory of Polymer Materials Engineering, Sichuan University, Chengdu 610065, P. R. China; and **Yongqin Zhang**, College of Chemical Engineering, Qingdao University of Science & Technology, 266042, Qingdao, P. R. China, E-mail: zhaojian@qust.edu.cn (J. Zhao), zyq0205@qust.edu.cn (Y. Zhang). https://orcid.org/0000-0002-7788-9026 (J. Zhao)
Changjiu Sun, Key Laboratory of Rubber-Plastics Ministry of Education/Shandong Provincial Key Laboratory of Rubber-Plastics, Qingdao University of Science & Technology, 266042, Qingdao, P. R. China; and Key Laboratory of Adv. Energy Mater. Chemistry (Ministry of Education), Renewable Energy Conversion and Storage Center (RECAST), College of Chemistry, Nankai University, 300071, Tianjin, P. R. China
Junli Wei, Yuanzhi Jiang and Mingjian Yuan, Key Laboratory of Adv. Energy Mater. Chemistry (Ministry of Education), Renewable Energy Conversion and Storage Center (RECAST), College of Chemistry, Nankai University, 300071, Tianjin, P. R. China
Yilong Wang, Key Laboratory of Rubber-Plastics Ministry of Education/Shandong Provincial Key Laboratory of Rubber-Plastics, Qingdao University of Science & Technology, 266042, Qingdao, P. R. China
Haiqing Hu and Xin Wang, Key Laboratory of Rubber-Plastics Ministry of Education/Shandong Provincial Key Laboratory of Rubber-Plastics, Qingdao University of Science & Technology, 266042, Qingdao, P. R. China; School of Materials Science and Engineering, Qilu University of Technology (Shandong Academy of Sciences), Jinan 250353, P. R. China; Key Laboratory of Organosilicon Chemistry and Material Technology of Ministry of Education, Hangzhou Normal University, Hangzhou 311121, P. R. China; and State Key Laboratory of Polymer Materials Engineering, Sichuan University, Chengdu 610065, P. R. China

Abstract: All-inorganic $CsPbBr_3$ perovskite is an attractive emission material for high-stability perovskite light-emitting diodes (PeLEDs), due to the high thermal and chemical stability. However, the external quantum efficiencies (EQEs) of $CsPbBr_3$ based PeLEDs are still far behind their organic–inorganic congeners. Massive defect states on the surface of $CsPbBr_3$ perovskite grains should be the main reason. Lewis base additives have been widely used to passivate surface defects. However, systematic investigations which relate to improving the passivation effect via rational molecule design are still lacking. Here, we demonstrate that the $CsPbBr_3$ film's optical and electrical properties can be significantly boosted by tailoring the hardness–softness of the Lewis base additives. Three carboxylate Lewis bases with different tail groups are selected to *in-situ* passivate $CsPbBr_3$ perovskite films. Our research indicates that 4-(trifluoromethyl) benzoate acid anion (TBA^-) with the powerful electron-withdrawing group trifluoromethyl and benzene ring possesses the softest COO^- bonding head. TBA^- thus acts as a soft Lewis base and possesses a robust combination with unsaturated lead atoms caused by halogen vacancies. Based on this, the all-inorganic $CsPbBr_3$ PeLEDs with a maximum EQE up to 16.75% and a half-lifetime over 129 h at an initial brightness of 100 cd m^{-2} is thus delivered.

Keywords: all-inorganic perovskite; $CsPbBr_3$; Lewis base; perovskite light-emitting diodes.

1 Introduction

Metal halide perovskite films fabricated by solution-processed method is promising candidates for the next-generation display and light-emitting devices contributed to their high photoluminescence quantum yield (PLQY), tunable bandgap, excellent color purity, and simple preparation process. At present, green and near-infrared emission perovskite light-emitting diodes

(PeLEDs) based on organic–inorganic metal halide perovskites have both achieved external quantum efficiency (EQE) exceeding 20% [1–5], comparable to the commercial organic light-emitting diodes (OLEDs) and quantum dots light-emitting diodes (QLEDs). However, the organic–inorganic hybrid perovskites employed methylamine (MA^+) or formamidine (FA^+) as 'A-site' cations inevitably occur severe thermal degradation under the operation conditions. This can be attributed to the poor thermal stability of these organic cations [6, 7]. The low operational stability thus severely restricts the application of the organic–inorganic hybrid PeLEDs. All-inorganic $CsPbBr_3$ perovskites show higher tolerance to Joule heating under operation conditions than its analogs such as $MAPbBr_3$ and $FAPbBr_3$, for its high thermal degradation temperature. Even though $CsPbBr_3$ materials show potential in extending the operating lifetime of PeLEDs, the EQEs of $CsPbBr_3$ PeLEDs are still far behind the organic–inorganic hybrid analogs [8–13]. The disappointing EQEs of $CsPbBr_3$ PeLEDs can be ascribed to the high defect state density and poor quality of the $CsPbBr_3$ films. $CsPbBr_3$ features a rapid crystallization process due to its poor solubility and low nucleation concentration. The resulting film thus shows reduced crystallinity and massive defect states.

Unsaturated lead atoms caused by halogen vacancies are the common crystal defect in perovskite materials. Halogen vacancies reduce the energy level of Pb 6*p* orbits and introduce deep-level states in the bandgap, which are widely regarded as nonradiative recombination sites [14–16]. Moreover, the halogen vacancies exhibit high affinity to various nucleophilic molecules such as oxygen or moisture, thus accelerating the perovskite degradation and deteriorating the film's environmental stability [17]. Lewis base molecules, as electron–pair acceptors, can effectively coordinate with unsaturated lead atoms through forming acid–base complexes. So far, typical Lewis base molecules such as pyridine, thiophene [18], ethylenediamine (EDA) [19], and trioctylphosphine oxide (TOPO) [2] have been used to passivate perovskite solar cells or LED devices, which achieve significant photoelectric properties improvement. However, most of these passivation strategies were carried out through a post treatment process, where a considerable amount of defect states still existed inside the resulting films. Moreover, the commonly used Lewis base molecules show low resistance of Joule heating, thus limiting their application in high-temperature fabrication technologies and reducing their long-term operational stability.

Anionic X-type ligands, such as alkylphosphonates, sulfonates, and carboxylates [20–22], represent as an important category of Lewis base. These anionic X-type ligands have been widely used in the synthesis of perovskite nanocrystals and revealed efficient passivation due to the coordination with unsaturated lead. Meanwhile, anionic X-type ligands feature high thermal stability, thus demonstrating compatibility for fabricating PeLEDs with long-term operational stability. However, few researches reported the relationship between the molecule structure of anionic X-type ligands and corresponding passivation effect. To reveal the underlying connection and propose a universal strategy for designing the additive molecules, we herein introduced three carboxylate sodium salts with different molecule structures into the $CsPbBr_3$ perovskite precursor for *in-situ* passivating the film's defect states. These carboxylate sodium salts include hexanoic acid sodium salt (HAS), benzoic acid sodium salt (BAS) and 4-(trifluoromethyl) benzoate acid sodium salt (TBAS). We found that 4-(trifluoromethyl) benzoate acid anion (TBA^-) contains powerful electron-withdrawing groups exhibits the most efficient passivation effect, compared to hexanoic acid anion (HA^-) or benzoic acid (BA^-). The soft base character of TBA^- decides the robust coordination between TBA^- and soft acid center Pb^{2+}, based on the Hard–Soft Acid–Base (HSAB) theory [23]. At the same time, we also found that introducing TBAS into the precursor leads to a smooth and pinhole-free film, confirming the role of TBAS in increasing the $CsPbBr_3$ nuclei density and inhibiting grain overgrowth. The multifunctional passivation effect of TBAS thus synergistically improves the optical and electrical performances of $CsPbBr_3$ film. Consequently, the all-inorganic $CsPbBr_3$ PeLED fabricated by a simple solution method achieves an EQE of 16.75%. More importantly, a half-lifetime up to 129 h is obtained at an initial brightness of 100 cd m^{-2}.

2 Results and discussions

2.1 DFT simulation of Lewis bases additives

As we know, unsaturated lead atom, which possesses large polarizability, actually acts as a soft acid [22, 24]. This means that, according to the HSAB theory, Lewis bases with soft binding heads should have more robust coordination ability with the unsaturated lead atoms, compared to hard Lewis bases. Considering that soft–soft interaction possesses stronger covalent bond characters, we conclude that the carboxylate anions with different hardness–softness will affect their passivation effect. Theoretically, soft and polarizable molecules can be obtained by narrowing their HOMO–LUMO gaps. This can be explained by a widely accepted principle: molecules with a narrow

HOMO–LUMO gap have low stability and electron-donating/withdrawing ability, are easily polarized, i.e., they exhibit soft properties [25–27]. Here, HOMO refers to the highest occupied molecule orbital and LUMO refers to the lowest unoccupied molecule orbital. Thus, the passivation effects of the anionic X-type ligands can be modified by tuning their electronic band structures.

Three carboxylate sodium salts, HAS, BAS, and TBAS, with different electron-withdrawing or -donating groups are selected to passivate the all-inorganic $CsPbBr_3$ films. These three Lewis bases possess the same binding head group (carboxylate group), but own different tail group respectively. Taken the BAS as reference, we selected HAS by replacing the phenyl group with donating groups (alkyl group) and TBAS with additional electron-withdrawing groups (trifluoromethyl group, CF_3). To demonstrate the systematic difference of these Lewis bases, we firstly used the density functional theory (DFT) with a frequently-used functional, B3LYP, to simulate the ground-state geometries and electrostatic potentials (ESP) of these anions. As shown in Figure 1a, the carboxylate anion (COO^-) binding heads appeal to the higher electron density (exhibited in red area), whereas the alkyl chains contain lower electron density (in blue area). When changing the tail group from saturated alkyl chain to benzene ring, the electron cloud is partially dispersed on the benzene ring leading to the reduction of charge density in the COO^- head group. Further linking a tail trifluoromethyl group will aggravate the delocalization of the electron cloud. We then extracted the HOMO and LUMO distributions of these three anions. As illustrated in Figure 1b, the HOMO levels are mainly located on the O atoms of the COO^- binding head, while LUMO levels are primarily located on the C atoms. Obviously, compared with the others, we found that after introducing the electron-withdrawing groups (CF_3) into Lewis base, the HOMO–LUMO gaps dropped from 4.89 eV for HA^- to 3.54 eV for TBA^- (Table S1). We also calculated another Lewis bases with a $-SO_3^-$ or $-P(OH)OO^-$ binding heads, however, these Lewis bases anion show wider gap compared to TBA^-. Since the electronegativity of C is smaller than that of O, the change of LUMO level thus more obvious than that of HOMO when introducing electron-withdrawing or -donating groups. The electron-donating groups can increase the energy levels of HOMO and LUMO and make the LUMO energy level increase to a greater extent, thereby increasing the HOMO–LUMO gap. While the electron-withdrawing group lowers the LUMO energy level to a greater extent, thus reducing the HOMO–LUMO gap. In TBA^-, benzene ring and trifluoromethyl group possess strong electron-withdrawing ability narrowed the HOMO–LUMO gap and led the softest COO^- binding head.

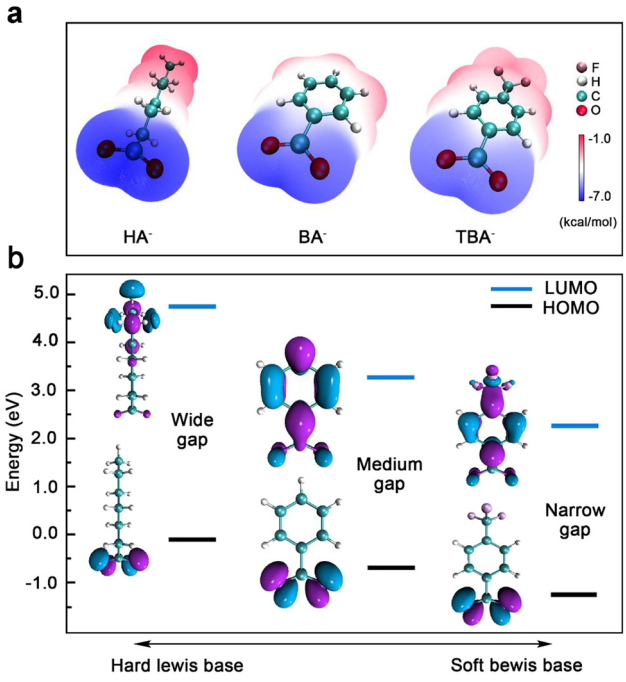

Figure 1: Molecule structures of different carboxylate anions. (a) Molecule structures and electrostatic potentials (ESPs) of the HA^-, BA^- and TBA^-. (b) HOMO and LUMO molecule orbitals of HA^-, BA^- and TBA^-.

2.2 Structural characterizations of the perovskite films

We then introduced these three carboxylate sodium salts into the all-inorganic $CsPbBr_3$ precursor systems and investigated their passivation effect. $CsPbBr_3$ perovskite films were prepared by a simple one-step spin coating method (Figure S1). To evaluate the different coordination abilities between carboxylates and unsaturated lead, we carried out X-ray photoelectron spectroscopy (XPS) measurements and investigated the compositions and corresponding chemical states of different films. Figure 2a and b demonstrate the XPS spectra for Pb 4*f* and Br 3*d*. As shown in Figure 2a, XPS spectrum of the original $CsPbBr_3$ film shows characteristic peaks of Pb $4f_{5/2}$ and Pb $4f_{7/2}$ at 143.4 and 138.3 eV [10, 28], respectively. While in the TBAS-containing film, shifts about 0.3 eV of these peaks toward high binding energy can be observed. However, such movement reduced to 0.2 eV in the film incorporated with BAS and almost negligible in the film incorporated with HAS. These movements in the Pb 4*f* spectra can be explained by the lone electron pair on the oxygen atom of the COO^- group contributing to the empty orbital on unsaturated lead, as has been reported in previous works [10]. The combination between COO^- and unsaturated lead

increases the energy of the Pb 6*p* states, making photogenerated electrons on the conduction band less likely to fall into the deep level, and improving the optical performance of the perovskite film. In addition, in the original and HAS-containing $CsPbBr_3$ perovskite films, additional shoulder peaks around 141.7 eV can be observed, which correspond to the metallic Pb [28]. These peaks disappeared in the perovskite films incorporated with BAS and TBAS, illustrating the coordination ability of BAS and TBAS with unsaturated lead. Shifts toward high binding energy have also been seen in the Br 3*d* spectra (Figure 2b), indicating the formation of the stabler perovskite phase [10, 29, 30]. Inversely, for HA^- with long-chain alkyl groups feature electron-donating ability, the widest HOMO–LUMO gap thus makes the hardest binding head. The mismatch of hard–soft leads to the weakest combining capacity. The robust coordination between TBAS and unsaturated lead was also verified by Fourier transform infrared (FTIR) and ^1H nuclear magnetic resonance (NMR) spectroscopy (Figures 2 and 3). The red-shift of COO^- group stretching vibration peak and downfield-shift of proton resonance signals were also observed.

X-ray diffraction (XRD) characterizations exhibit crystallization properties of these $CsPbBr_3$ films. XRD patterns of the original $CsPbBr_3$ film and the films incorporated with different carboxylate sodium salts are shown in Figure 2c. All films show obvious diffraction peaks locate at 15.4°, 21.8°, and 30.8° correspond to the (100), (110), and (200) crystal planes, consistent with the positions reported in the previous literatures [10, 11]. Then, once added the HAS,

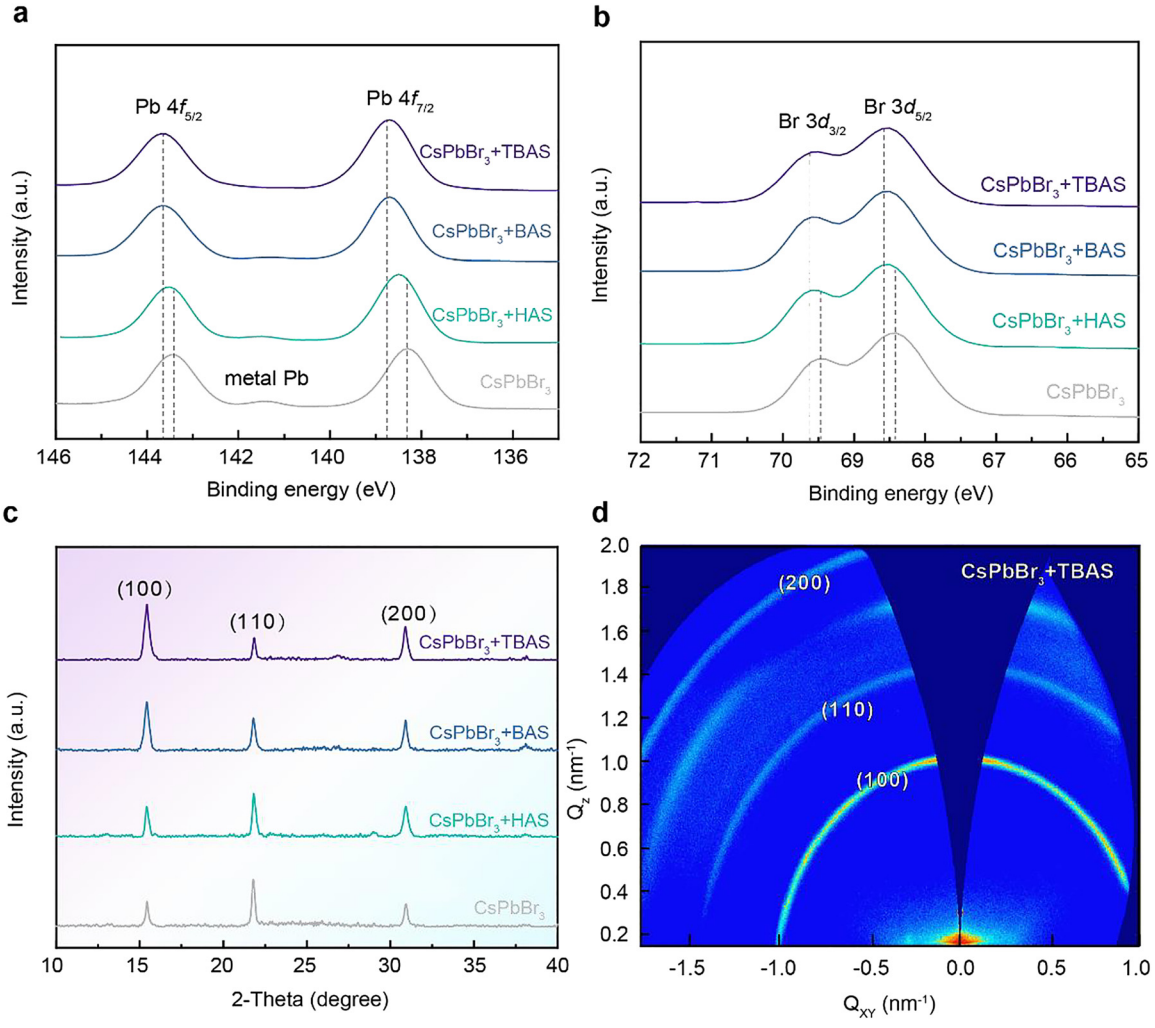

Figure 2: Structural characterizations of the $CsPbBr_3$ perovskite films.
(a) Pb 4*f*, (b) Br 3*d* X-ray photoelectron spectroscopy (XPS) spectra, and (c) X-ray diffraction (XRD) patterns of the original $CsPbBr_3$ film and $CsPbBr_3$ films incorporated with hexanoic acid sodium salt (HAS), benzoic acid sodium salt (BAS), and 4-(trifluoromethyl) benzoate acid sodium salt (TBAS). (d) Grazing-incidence wide-angle X-ray scattering (GIWAXS) pattern of the TBAS-containing $CsPbBr_3$ films.

BAS, or TBAS, the diffraction peaks corresponding to (100) and (200) planes increased gradually, while the diffraction peaks corresponding to the (110) reflection planes decreased. This change can be explained by the improvement of the crystallinity and the adjustment of preferential orientation. Compared with the original $CsPbBr_3$ film, about a twice-fold increase of the (100) and (200) diffraction peaks in the TBAS-containing film indicates that TBAS has a significant effect on improving the film's crystallinity. We also calculated average thicknesses perpendicular to the (100) plane of different $CsPbBr_3$ films and found that the average thicknesses of original $CsPbBr_3$ film up to 45.3 nm, but decreased to 22.6 nm of TBAS-containing $CsPbBr_3$ film (Supplementary Method 1). Furthermore, we did not notice the significant movement of the diffraction peak in any case. Thus, we concluded that carboxylate and Na^+ anions could not insert into the grain lattice or induced the undesired phase transformation. Grazing-incidence wide-angle X-ray scattering (GIWAXS) pattern of the TBAS-containing film is also shown in Figure 2d. The uniform Debye–Scherrer rings indicate that the perovskite crystallites were isotopically oriented in the film [31].

2.3 Morphological studies of the perovskite films

Atomic force microscopy (AFM) images were used to characterize the morphologies of original and different carboxylate sodium salts modified $CsPbBr_3$ films. As shown in Figure 3a, the original $CsPbBr_3$ perovskite film features low surface coverage and large grain size, resulting in a root mean square roughness (r.m.s.) up to 9.8 nm. This is consistent with previous reports [10, 11], and can be explained by the fact that the limited solubility of the $CsPbBr_3$ precursor leads to extremely fast and inhomogeneous crystallization of $CsPbBr_3$ perovskite. While for the $CsPbBr_3$ perovskite film incorporated with carboxylate sodium salts, increased surface coverage, reduced grain size and decreased average roughness were observed. The r.m.s. of the $CsPbBr_3$ incorporated with HAS, BAS, and TBAS extracted from AFM images were 5.5, 3.7, and 1.9 nm, respectively (Figure 3b–d). The same trend is also observed in the scanning electron microscopy (SEM) images (Figure S4). We first attributed the improved film quality to the coordination between $[PbBr_6]^-$ clusters and carboxylate sodium salts. Such coordination slowed down the crystallization process of $CsPbBr_3$ perovskite, facilitating the uniform grain growth and improving the film crystallinity [32, 33]. Besides, carboxylate sodium salts additives also increased the heterogeneous nucleation sites in the precursor, thus benefiting the formation of perovskite film with small grain size and high surface coverage. Moreover, previous works have reported that the alkali metal ions can occupy the "A-site" on the surface of the perovskite grain, thus act as spacers and inhibit the overgrowth of the grain [34]. This is similar to organic cation spacers such as phenethylamine (PEA) or butylamine (BA) commonly used in low-dimensional perovskites. Sodium ions with small ion radius are hard to incorporate into the perovskite lattice, but tend to occupy the "A-site" on the grain surface. The uniform distribution of sodium has also been confirmed by the DES images (Figure S5). The reduced perovskite grain size enhanced the confined effect of the electron–hole pairs, thus suppressing electron–hole pairs decoupling into free carriers. We stress that tightly bound electron–hole pairs are essential to improve optical performance, considering that free carriers are more likely to dissociate to the grain boundary and trapped by the defect states. On the other hand, improved film quality can also eliminate carrier shunting paths and reduce undesired large leakage current in the device, which is also beneficial to the device's electrical performance improvement.

2.4 Optical characterizations of the perovskite films

To explore the films' optical properties, steady-state PL and UV–Vis absorbance spectra were collected and demonstrated in Figure 4a and Figure S6. All films showed similar absorption edges and PL peaks around 520 nm, corresponding to the optical bandgap of ~2.38 eV. Obviously, compared to the original $CsPbBr_3$ film, the $CsPbBr_3$ perovskite films incorporated with carboxylate sodium salts showed higher PL intensity. The average PLQY increased from 11% of the original $CsPbBr_3$ film to 16, 42, and 62% of the films incorporated with HAS, BAS, and TBAS (Figure 4b and Figure S7), respectively, proving that the films incorporated with carboxylate sodium salts have higher radiation recombination efficiency. Time-resolved PL (TRPL) spectra were thus recorded to investigate the carrier recombination behaviors of these films. As shown in Figure 4c, an average carrier lifetime (τ_{avg}) of 31 ns is observed for the original $CsPbBr_3$ perovskite film. In comparison, τ_{avg} of 33 ns for HAS-containing film, 69 ns for BAS-containing film, and 74 ns for TBAS-containing films indicated the improved stability of electron–hole pairs. The reduced defect state density of the perovskite film should be the reason for optical performance improvement. The most extended carrier lifetime in the TBAS-containing $CsPbBr_3$ perovskite film thus means the lowest density of

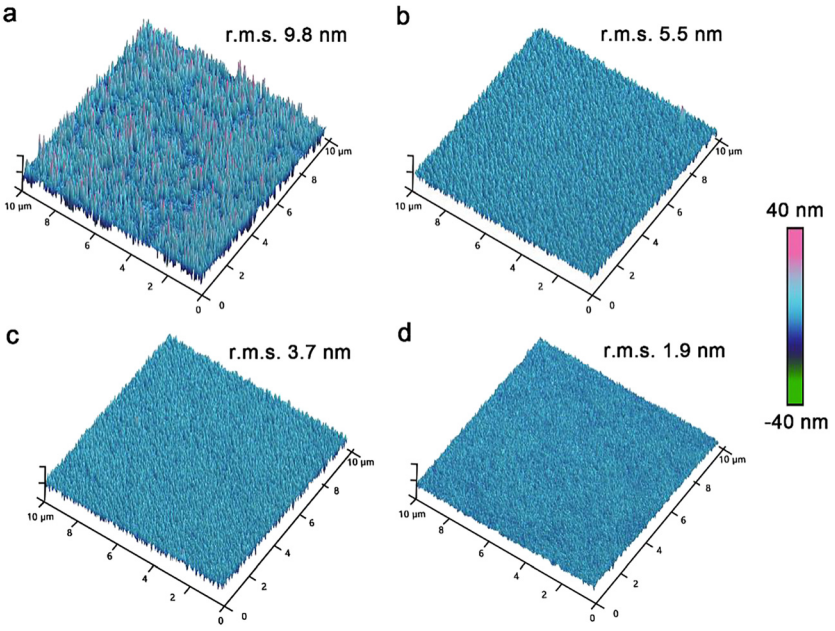

Figure 3: Morphological studies of the $CsPbBr_3$ perovskite films.
Atomic force microscopy (AFM) images of (a) original $CsPbBr_3$ film and $CsPbBr_3$ films incorporated with (b) hexanoic acid sodium salt (HAS), (c) benzoic acid sodium salt (BAS), and (d) 4-(trifluoromethyl) benzoate acid sodium salt (TBAS), respectively.

defect states, corresponding to the most robust coordination ability of TBA^- anion with unsaturated lead. We then used transient absorption (TA) spectroscopy to further understand the carrier dynamics of the original and TBAS-containing $CsPbBr_3$ perovskite films. All samples were excited by a 365-nm pump pulse, by monitoring the absorption of the probe and reference lights, the bleach signal of the film can be obtained [35]. Compared with the original film (Figure 4d), a smaller redshift of the transient bleach was observed in the TBAS-containing film (Figure 4e). Here, we identified the redshift of the transient as the band tail state filling process [10, 36]. That is, TBAS additive eliminated undesirable band tail states effectively. TA traces as a function of decay time were also shown in Figure 4f. Here the τ_e was defined as the time when the TA population decays to 1/e of its initial intensity. Under the same excitation intensity, the extracted τ_e of the TBAS-containing film was 392 ps, much larger than the original film of 126 ps. The increased photobleaching delay time proves the decrease of the carrier quenching sites in the TBAS-containing film [36].

To quantify the passivation effect of carboxylate sodium salts, we further adopted a widely reported spatial charge-limited current (SCLC) model to extract the films' defect state densities (Figure S8) [37]. Defect state densities of 1.52×10^{17}, 1.36×10^{17}, 7.26×10^{16}, and 6.01×10^{16} cm^{-3} were extracted for original $CsPbBr_3$ films and $CsPbBr_3$ films incorporated with HAS, BA, and TBAS, respectively. Such a trend is in good agreement with the results of optical characterization. Therefore, both optical and electrical measurements confirmed the passivation effect of carboxylate sodium salts. The TBAS-containing film exhibits optical and electrical performances with the most significant improvements and minimum defect state densities, stemming from the most robust combination between TAB^- and unsaturated lead.

2.5 EL performances of the PeLEDs

Encouraged by the improved optical and electrical properties, we thus built different $CsPbBr_3$ PeLED devices to investigate the EL performance of the obtained films. All devices were based on an ITO/NiO_x/PVK/PFNBr/Perovskite active layer/TPBi/LiF/Al architecture. The corresponding energy level diagram of the PeLEDs is shown in Figure 5a [14, 38]. Here, the *p*-type NiO_x was used as a hole-transport/electron-blocking layer, owing to their excellent humidity and thermos-stability. An ultrathin PVK/PFNBr bilayer structure was employed to passivate nickel oxyhydroxide defects and modify film wettability [39]. While the *n*-type TPBi were used as a hole transport layer. Figure 5b shows the typical EL spectra of the devices located at 520 nm. We noticed that the emission peak did not show obvious changes in either case. The TBAS-containing device offers the narrowest FWHM of 19 nm. We ascribe this to the fact that TBAS inhibited the low energy transitions by eliminating interstitial bands caused by defects and vacancies. The current density–voltage (*J*–*V*), luminance–voltage (*L*–*V*) and EQE–current density (*EQE*–*J*) curves of different $CsPbBr_3$ PeLED devices are shown in Figure 5c–e. Detailed performance indicators

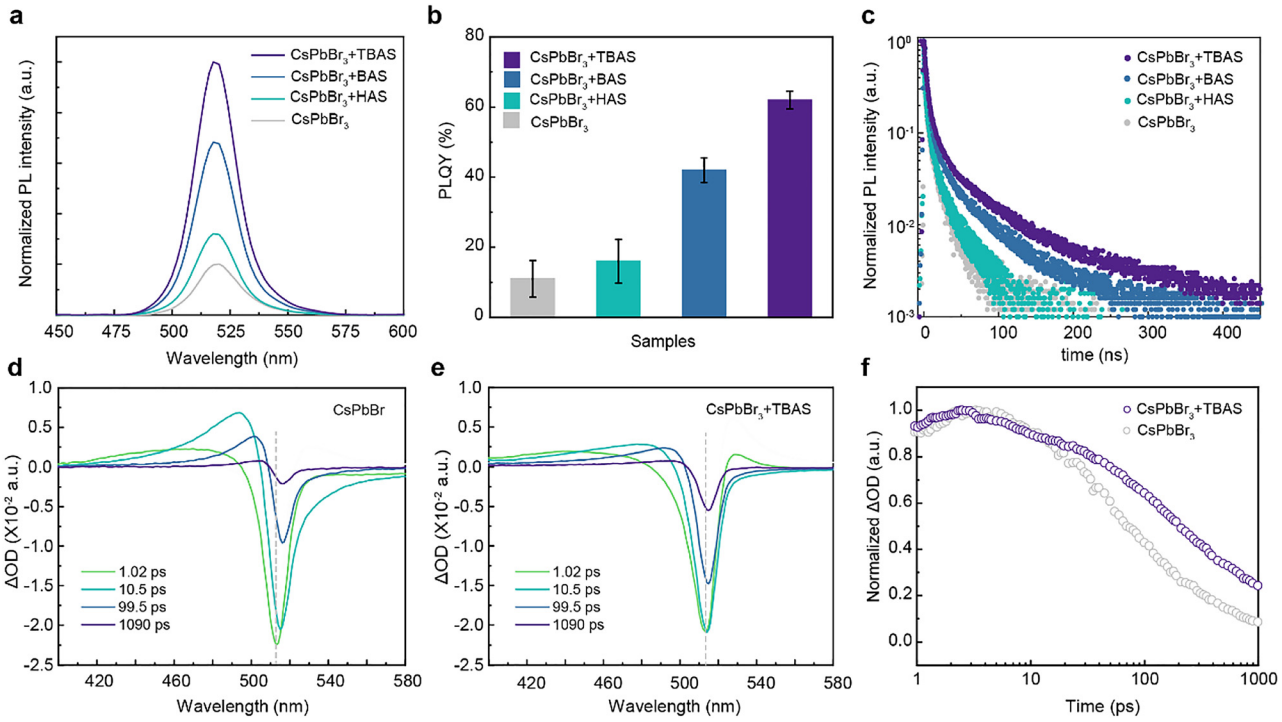

Figure 4: Optical characterizations of the $CsPbBr_3$ perovskite films.
(a) Steady-state PL spectra, (b) photoluminescence quantum yield (PLQY) values, and (c) time-resolved PL (TRPL) spectra of original $CsPbBr_3$ film and $CsPbBr_3$ films incorporated with hexanoic acid sodium salt (HAS), benzoic acid sodium salt (BAS), and 4-(trifluoromethyl) benzoate acid anion (TBA), respectively. Transient absorption maps of the (d) original and (e) 4-(trifluoromethyl) benzoate acid sodium salt (TBAS)-containing $CsPbBr_3$ films. (f) Transient absorption (TA) decay kinetics of the original and TBAS-containing $CsPbBr_3$ films.

for each device were tabulated in Table S2. As expected, compared with the devices based on the original $CsPbBr_3$ film or HAS/BAS-containing $CsPbBr_3$ films, the TBAS-containing PeLED exhibits lower current density and higher brightness. A maximum luminance value of 37,860 cd m^{-2} was obtained at 6.4 V. As a result, the TBAS-containing PeLED yielded a high EQE up to 16.75% (Figure S9), while the original PeLED showed an EQE of only 2.08% and maximum luminance of 10,550 cd m^{-2}. Operational stabilities of the PeLEDs were also measured (Figure 5f and Figure S10). A half-lifetime over 129 h (T_{50}, the time when luminescence decay to half of the initial value) at an initial luminescence of 100 cd m^{-2} was achieved in TBAS-containing PeLED. This result represents one of the most efficient and stable $CsPbBr_3$ PeLED up to now [10, 40, 41]. As a contrast, original devices show a low T_{50} of 19 h. The impressive operational stability can be attributed to the TBAS passivation process which delivers a smooth and low defect density film, which further suppresses the nonradiative recombination and eliminates the ion migration channels. The improved film stability also confirmed by the temperature-dependent conductivity measurements, where obviously increased ion migration activation energies can be extracted in the TBAS-containing film (Figure S11).

3 Conclusion

In summary, we provide a strategy to modify the defect passivation effect by tailoring the hardness–softness of Lewis base additives. Our result demonstrates that anionic Lewis base TBA^-, containing electron-withdrawing groups, possesses a soft carboxylate anion (COO^-) binding head. TBA^- thus coordinates with unsaturated lead robustly, since the soft acid feature of lead atoms. In addition, we propose that sodium ions occupied the A site center on the surface of perovskite and act as spacers. Taking advantage of the above findings, the TBAS-containing $CsPbBr_3$ film with both high optical and electrical properties were obtained. Based on this film, we are able to deliver an all-inorganic $CsPbBr_3$ PeLED with an EQE of 16.75% and a high half-lifetime up to 129 h. Our work provides useful insights for designing the Lewis base additives rationally, and represents an important step towards the commercialization of the PeLED devices.

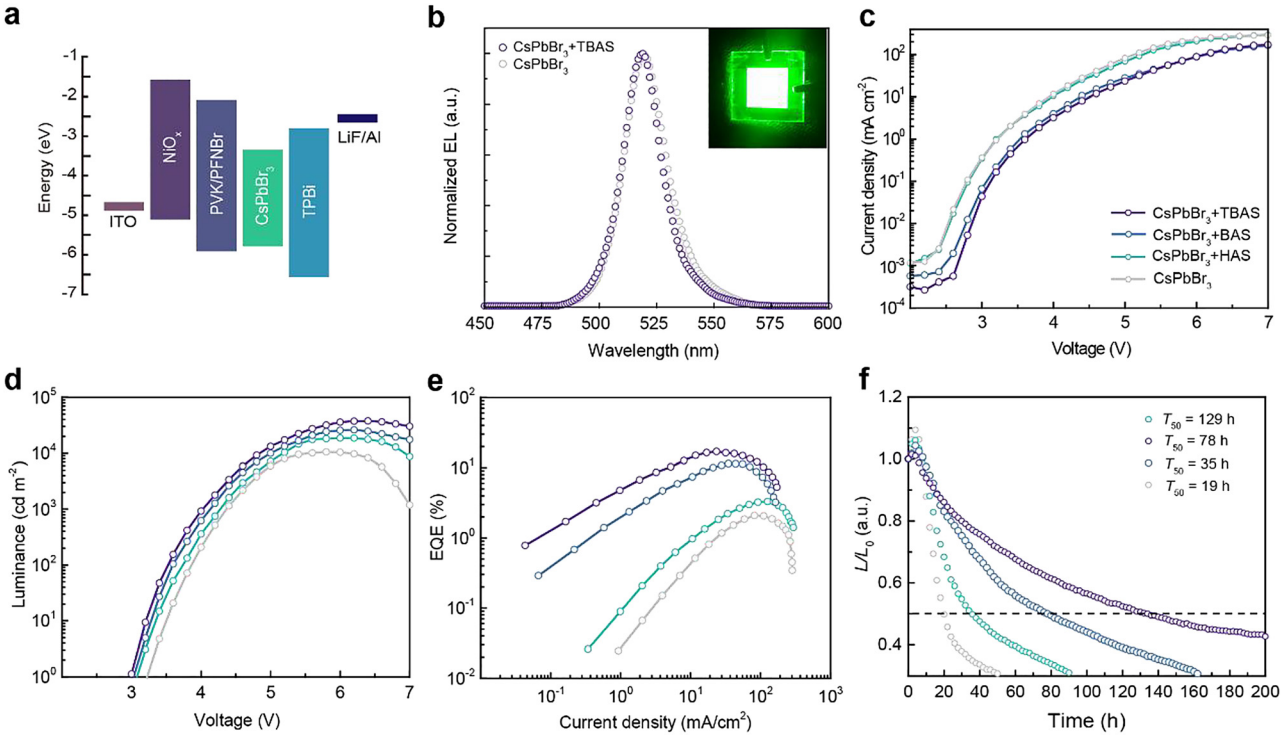

Figure 5: Electroluminescence (EL) performances characterization of the $CsPbBr_3$ PeLEDs.
(a) Energy level structure of each functional layer in the PeLED device. (b) EL spectra of original and 4-(trifluoromethyl) benzoate acid sodium salt (TBAS)-containing $CsPbBr_3$ PeLEDs, the inserted picture is the TBAS-containing device operated under biased voltage of 4.0 V. (c) *J–V*, (d) *L–V*, and (e) *EQE–J* curves of original $CsPbBr_3$ PeLED and $CsPbBr_3$ PeLEDs incorporated with hexanoic acid sodium salt (HAS), benzoic acid sodium salt (BAS) and 4-(trifluoromethyl) benzoate acid sodium salt (TBAS), respectively. (f) The stability measurement at an initial luminance of 100 cd m^{-2} for different $CsPbBr_3$ PeLEDs.

4 Experimental section

4.1 Materials

CsBr (99.999%), $PbBr_2$ (99.999%), Nickel(II) nitrate hexahydrate ($Ni(NO_3)_2{\cdot}6H_2O$, 99.999%) hexanoic acid sodium salt (HAS, 99.0%), benzoic acid sodium salt (BAS, 99.0%), and polyethylene glycol (PEG) were purchased from Sigma-Aldrich. 4-(trifluoromethyl) benzoate acid sodium salt (TBAS, 99.0%) was purchased from J&K Chemical. Poly(9-vinylcarbazole) (PVK), poly[(9,9-bis (3′-((*N*,*N*-dimethyl)-*N*-ethylammonium)-propyl)-2,7-fluorene)-alt-2,7-(9,9-dioctylfluorene)] (PFNBr), (1,3,5-benzinetriyl)-tris(1-phenyl-1-*H*-benzimidazole)) (TPBi), and LiF (99.99%) were purchased from Lumtech Corp. All the chemical materials were directly used without any further purifications.

4.2 Perovskite film fabrication

The perovskite precursor solutions were prepared by dissolving CsBr, $PbBr_2$ and carboxylate sodium salt in dimethyl sulfoxide (DMSO) with a molar ratio of 1.2:1:0.08, the concentration of $PbBr_2$ was kept at 0.25 M. A small amount of PEG with 1.5 wt% respect to $CsPbBr_3$ was also added in the precursor. All perovskite precursor solutions were filtered by a PTFE filter before using. The perovskite films were obtained in the glove box by spin-coating method at 1000 r.p.m. for 5 s and 4000 r.p.m. for 80 s. After the spin-coating process, the perovskite films were annealed at 100 °C for 5 min.

4.3 NiO_x hole transport layer fabrication

The NiO_x hole transport layer was prepared by an improved high-temperature sol–gel method [14]. 0.873 g of $Ni(NO_3)2{\cdot}6H_2O$ and 0.2 mL of ethylenediamine were dissolved in 3 mL of 2-methoxyethanol solution and stirring for 30 min. Then the precursor was spin-coated on clean and O_2 plasma treated ITO substrate at a speed of 2000 r.p.m. for 40 s. After the spin coating process, the films were firstly annealed in ambient at 80 °C for 2 min, and then transferred in the muffle furnace for another 60 min at 400 °C.

4.4 LEDs fabrication

After annealing, the ITO/NiO_x substrates were treated with O_2 plasma for 5 min and then transferred to a nitrogen-filled glovebox. A PVK solution dissolved in chlorobenzene with a concentration of 2 mg/mL was spin-coated on the NiO_x layer at a speed of 4000 r.p.m., followed

by annealing at 130 °C for 15 min. To improve the wettability of the PVK layer, a PFNBr solution dissolved in methanol with a concentration of 1 mg/mL was also spin-coated on the PVK layer, with a speed of 4000 r.p.m., and annealed at 70 °C for 2 min. After that, the perovskite film was deposited on the PFNBr layer. Finally, TPBi (40 nm), LiF (1.0 nm), and metal Al (150 nm) were deposited through thermal evaporation under a vacuum of $<1 \times 10^{-4}$ Pa.

4.5 Characterizations

The simulations were performed using a DFT method as implemented in the Gaussian 09 package. Ground-state geometries and molecule orbital energy levels of carboxylate anions were calculated at the B3LYP/6-31G* level. The UV–Vis absorption spectra were recorded using the LAMBDA 950 UV/Vis/NIR spectrophotometer. XPS measurements were carried out in a PHI 5000C EHASA X XPS (MgKα, $h\nu$ = 1253.6 eV) system. The Bruker D8 X-ray diffractometer (Cu Kα, λ = 1.5406 Å, 40 kV, 100 mA) was used to characterize the crystal structure of the perovskite films at a scanning rate of 10° min^{-1}, with a step size of 0.02°. Field emission SEM (JSM-7500F, JEOL), was used to observe the surface morphology of the perovskite film at an acceleration voltage of 5.0 kV. The AFM tests were carried out using an atomic force microscope (Dimension Icon, Bruker) in a noncontact mode. The photoluminescence properties of the perovskite films were measured by a fluorescence spectrophotometer (FS5, Edinburghinstruments), during the test, the perovskite films were spin-coated on the 2×2 cm^2 quartz glass. The steady-state PL spectra and PLQY of the films were recorded by exciting at 365 nm wavelength provided by a 450 W xenon lamp. The TRPL decay kinetic spectra were obtained by using a 365-nm laser as the excitation source. The TA measurements were carried out on a Helios pump-probe system (Ultrafast Systems LLC) coupled with an amplified femtosecond laser system (Coherent, 35 fs, 1 kHz, 800 nm). FTIR spectra were recorded under attenuated total reflectance (ATR) mode on a Nicolet iS50 spectrometer. ^{1}H NMR spectra were recorded in DMSO-d6 solvent by using a Bruker 400 MHz NMR spectrometer. Temperature-dependent conductivity measurements were carried out in a Lakeshore probe station incorporate with a heater under a vacuum of 10^{-4} pa. A Keithley 2400 was used for recording voltage-current responses. For electroluminescence measurement, all PeLED devices were measured in the nitrogen-filled glove box using an integrated system consisting of a digital source meter (Keithley 2400), a spectrometer (QE65 Pro, Ocean Optics), and an optical fiber integrating sphere (FOIS-1-FL, Ocean Optics); the effective device area was 8.6 mm^2. All of the EL data was double-checked by a PR-735 spectroradiometer (Photo Research).

Author contributions: All the authors contributed to the preparation of the manuscript, and have accepted responsibility for the entire content of this submitted manuscript and approved submission.

Research funding: This work was partially funded by the National Natural Science Foundation of China (NSFC No. 51873096), the Natural Science Foundation of Shandong Province (Nos. ZR201807060363 and ZR2019MEM001), the Primary Research & Development Plan of Shandong Province (No. 2017GGX20132), the Opening Project of State Key Laboratory of Polymer Materials Engineering (Sichuan University) (Grant No. sklpme2020-4-04) and Open Research Fund (KFJJ2021007, KFJJ2021004, and KFJJ202005) of Key Laboratory of Organosilicon Chemistry and Material Technology of Ministry of Education.

Conflict of interest statement: The authors declare no conflicts of interest regarding this article.

References

[1] K. Lin, J. Xing, L. N. Quan, et al., "Perovskite light-emitting diodes with external quantum efficiency exceeding 20 per cent," *Nature*, vol. 562, no. 7726, pp. 245–248, 2018.

[2] B. Zhao, S. Bai, V. Kim, et al., "High-efficiency perovskite–polymer bulk heterostructure light-emitting diodes," *Nat. Photonics*, vol. 12, no. 12, pp. 783–789, 2018.

[3] W. Xu, Q. Hu, S. Bai, et al., "Rational molecular passivation for high-performance perovskite light-emitting diodes," *Nat. Photonics*, vol. 13, no. 6, pp. 418–424, 2019.

[4] Y. Cao, N. Wang, H. Tian, et al., "Perovskite light-emitting diodes based on spontaneously formed submicrometre-scale structures," *Nature*, vol. 562, no. 7726, pp. 249–253, 2018.

[5] C. Sun, Y. Jiang, M. Cui, et al., "High-performance large-area quasi-2D perovskitelight-emitting diodes," *Nat. Commun.*, vol. 12, no. 2207, pp. 1–11, 2021.

[6] Y. Jiang, J. Yuan, Y. Ni, et al., "Reduced-dimensional α-$CsPbX_3$ perovskites for efficient and stable photovoltaics," *Joule*, vol. 2, no. 7, pp. 1356–1368, 2018.

[7] B. Conings, J. Drijkoningen, N. Gauquelin, et al., "Intrinsic thermal instability of methylammonium lead trihalide perovskite," *Adv. Energy Mater.*, vol. 5, no. 15, p. 1500477, 2015.

[8] X. Liu, X. Y. Guo, Y. Lv, et al., "High brightness and enhanced stability of $CsPbBr_3$-based perovskite light-emitting diodes by morphology and interface engineering," *Adv. Opt. Mater.*, vol. 6, no. 24, p. 1801245, 2018.

[9] Y. Meng, M. Ahmadi, X. Y. Wu, et al., "High performance and stable all-inorganic perovskite light emitting diodes by reducing luminescence quenching at PEDOT:PSS/perovskites interface," *Org. Electron.*, vol. 64, pp. 47–53, 2019.

[10] H. R. Wang, X. Y. Zhang, Q. Q. Wu, et al., "Trifluoroacetate induced small-grained $CsPbBr_3$ perovskite films result in efficient and stable light-emitting devices," *Nat. Commun.*, vol. 10, no. 665, pp. 1–10, 2019.

[11] Y. C. Ling, Y. Tian, X. Wang, et al., "Enhanced optical and electrical properties of polymer-assisted all-inorganic perovskites for light-emitting diodes," *Adv. Mater.*, vol. 28, no. 40, pp. 8983–8989, 2016.

[12] H. Cho, C. Wolf, J. S. Kim, et al., "High-efficiency solution-processed inorganic metal halide perovskite light-emitting diodes," *Adv. Mater.*, vol. 29, no. 31, p. 1700579, 2017.

[13] C. Wu, Y. T. Zou, T. Wu, et al., "Improved performance and stability of all-inorganic perovskite light-emitting diodes by antisolvent vapor treatment," *Adv. Funct. Mater.*, vol. 27, no. 28, p. 1700338, 2017.

[14] K. H. Wang, Y. D. Peng, J. Ge, et al., "Efficient and color-tunable quasi-2D $CsPbBr_xCl_{3-x}$ perovskite blue light-emitting diodes," *ACS Photonics*, vol. 6, no. 3, pp. 667–676, 2019.
[15] S. A. Veldhuis, Y. F. Ng, R. Ahmad, et al., "Crown ethers enable room-temperature et ILI synthesis of $CsPbBr_3$ quantum dots for light-emitting diodes," *ACS Energy Lett.*, vol. 3, no. 3, pp. 526–531, 2018.
[16] J. Z. Song, T. Fang, J. H. Li, et al., "Organic-inorganic hybrid passivation enables perovskite QLEDs with an EQE of 16.48%," *Adv. Mater.*, vol. 30, no. 50, p. 1805409, 2018.
[17] L. N. Quan, D. Ma, Y. Zhao, et al., "Edge stabilization in reduced-dimensional perovskites," *Nat. Commun.*, vol. 11, no. 170, pp. 1–9, 2020.
[18] N. K. Noel, A. Abate, S. D. Stranks, et al., "Enhanced photoluminescence and solar cell performance via Lewis base passivation of organic–inorganic lead halide perovskites," *ACS Nano*, vol. 8, no. 10, pp. 9815–9821, 2014.
[19] S. Lee, J. H. Park, B. R. Lee, et al., "Amine-based passivating materials for enhanced optical properties and performance of organic–inorganic perovskites in light-emitting diodes," *J. Phys. Chem. Lett.*, vol. 8, no. 8, pp. 1784–1792, 2017.
[20] E. Yassitepe, Z. Yang, O. Voznyy, et al., "Amine-free synthesis of cesium lead halide perovskite quantum dots for efficient light-emitting diodes," *Adv. Funct. Mater.*, vol. 26, no. 47, pp. 8757–8763, 2016.
[21] D. Yang, X. Li, W. Zhou, et al., "$CsPbBr_3$ quantum dots 2.0: benzenesulfonic acid equivalent ligand awakens complete purification," *Adv. Mater.*, vol. 31, no. 30, p. 1900767, 2019.
[22] D. P. Nenon, K. Pressler, J. Kang, et al., "Design principles for trap-free $CsPbX_3$ nanocrystals: enumerating and eliminating surface halide vacancies with softer Lewis bases," *J. Am. Chem. Soc.*, vol. 140, no. 50, pp. 17760–17772, 2018.
[23] R. G. Pearson, "Hard and soft acids and bases," *J. Am. Chem. Soc.*, vol. 85, no. 22, pp. 3533–3539, 1963.
[24] Y. Tang, N. Yan, Z. Wang, et al., "Precursor solution volume-dependent ligand-assisted synthesis of $CH_3NH_3PbBr_3$ perovskite nanocrystals," *J. Alloys Compd.*, vol. 773, pp. 227–233, 2019.
[25] R. R. d. Silva, J. M. Santos, T. C. Ramalho, and J. D. Figueroa-Villar, "Concerning the FERMO concept and Pearson's hard and soft acid-base principle," *J. Braz. Chem. Soc.*, vol. 17, no. 2, pp. 223–226, 2006.
[26] Z. Zhou and G. P. Robert, "Activation hardness: new index for describing the orientation of electrophilic aromatic substitution," *J. Am. Chem. Soc.*, vol. 112, no. 15, pp. 5720–5724, 1990.
[27] E. C. Koch, "Acid-base interactions in energetic materials: I. The hard and soft acids and bases (HSAB) principle–insights to reactivity and sensitivity of energetic materials," *Propellants Explos. Pyrotech.*, vol. 30, no. 1, pp. 5–16, 2005.
[28] Z. B. Fang, W. J. Chen, Y. L. Shi, et al., "Dual passivation of perovskite defects for light-emitting diodes with external quantum efficiency exceeding 20%," *Adv. Funct. Mater.*, vol. 30, no. 12, p. 1909754, 2020.
[29] M. Liu, G. Zhong, Y. Yin, et al., "Aluminum-doped cesium lead bromide perovskite nanocrystals with stable blue photoluminescence used for display backlight," *Adv. Sci.*, vol. 4, no. 11, p. 1700335, 2017.
[30] J. K. Nam, S. U. Chai, W. Cha, et al., "Potassium incorporation for enhanced performance and stability of fully inorganic cesium lead halide perovskite solar cells," *Nano Lett.*, vol. 17, no. 3, pp. 2028–2033, 2017.
[31] M. Ban, Y. Zou, J. P. Rivett, et al., "Solution-processed perovskite light emitting diodes with efficiency exceeding 15% through additive-controlled nanostructure tailoring," *Nat. Commun.*, vol. 9, no. 3892, pp. 1–10, 2018.
[32] C. Gao, Y. Jiang, C. Sun, et al., "Multifunctional naphthol sulfonic salt incorporated in lead-free 2D tin halide perovskite for red light-emitting diodes," *ACS Photonics*, vol. 7, no. 8, pp. 1915–1922, 2020.
[33] X. Meng, J. Lin, X. Liu, et al., "Highly stable and efficient $FASnI_3$-based perovskite solar cells by introducing hydrogen bonding," *Adv. Mater.*, vol. 31, no. 42, p. 1903721, 2019.
[34] H. T. Chen, L. W. Fan, R. Zhang, et al., "Sodium ion modifying in-situ fabricated $CsPbBr_3$ nanoparticles for efficient perovskite light emitting diodes," *Adv. Opt. Mater.*, vol. 7, no. 21, p. 1900747, 2019.
[35] M. Yuan, L. N. Quan, R. Comin, et al., "Perovskite energy funnels for efficient light-emitting diodes," *Nat. Nanotechnol.*, vol. 11, pp. 872–877, 2016.
[36] B. Han, S. Yuan, T. Fang, et al., "Novel Lewis base cyclam self-passivation of perovskites without an anti-solvent process for efficient light-emitting diodes," *ACS Appl. Mater. Interfaces*, vol. 12, no. 12, pp. 14224–14232, 2020.
[37] D. Shi, V. Adinolfi, R. Comin, et al., "Low trap-state density and long carrier diffusion in organolead trihalide perovskite single crystals," *Science*, vol. 347, no. 6221, pp. 519–522, 2015.
[38] Z. Xiao, R. A. Kerner, L. Zhao, et al., "Efficient perovskite light-emitting diodes featuring nanometre-sized crystallites," *Nat. Photonics*, vol. 11, no. 2, pp. 108–115, 2017.
[39] Y. Zou, M. Ban, Y. Yang, et al., "Boosting perovskite light-emitting diode performance via tailoring interfacial contact," *ACS Appl. Mater. Interfaces*, vol. 10, no. 28, pp. 24320–24326, 2018.
[40] T. Wu, J. Li, Y. Zou, et al., "High-performance perovskite light-emitting diode with enhanced operational stability using lithium halide passivation," *Angew. Chem. Int. Ed.*, vol. 59, no. 10, pp. 4099–4105, 2020.
[41] L. Zhang, F. Yuan, J. Xi, et al., "Suppressing ion migration enables stable perovskite light-emitting diodes with all-inorganic strategy," *Adv. Funct. Mater.*, vol. 30, no. 40, p. 2001834, 2020.

Supplementary Material: The online version of this article offers supplementary material (https://doi.org/10.1515/nanoph-2021-0003).